Time Synchronization for Full-Duplex Communications

AAMER ALHAMWI
ZIYU LIU
MASTER´S THESIS
DEPARTMENT OF ELECTRICAL AND INFORMATION TECHNOLOGY
FACULTY OF ENGINEERING | LTH | LUND UNIVERSITY

Time Synchronization for Full-Duplex Communications

Master Thesis

By

Aamer Alhamwi and Ziyu Liu

Supervisor:
Minkeun Chung

Department of Electrical and Information Technology
Faculty of Engineering, LTH, Lund University
SE-221 00 Lund, Sweden

LUND UNIVERSITY

2019

Abstract

In-band full-duplex has emerged as an attractive solution for significantly enhancing the throughput of wireless communication systems by doubling the spectrum efficiency compared to conventional half-duplex systems. However, the existence of self-interference is a significant barrier to operate full-duplex systems. In order to cancel the self-interference by analog and digital solutions, time synchronization in digital domain is one of the most important elements in full-duplex systems.

The aim of this thesis is to present a time synchronization method for orthogonal frequency division multiplexing (OFDM) full-duplex transceiver based on Long Term Evolution (LTE) and validate its performance by MATLAB simulation. The proposed method acquires time offset information of both desired and self-interference signals in a full-duplex node to enhance the successful synchronization probability. To do this, a Zadoff-Chu sequence with a different root index is used for the primary synchronization signal (PSS) at each node. Further, we discuss about the application of different threshold values for the adaptive cross-correlation peak detection of two kinds of PSSs in a full-duplex node.

Acknowledgements

First of all, we would like to offer our special thanks to our supervisor Minkeun Chung whose motivation, support and encouragement throughout the course helped us to accomplish our project. Furthermore, we would like to express our prodigious appreciation to our professors and lecturers who provided us with valuable information in regards to our field of study.

We would also like to extend our thanks to our family, specially our parents who always supported and motivated us in our studies and their confidence in us has always played a key role in our success.

Aamer Alhamwi and Ziyu Liu

Contents

Abstract 2

Acknowledgements 3

Contents 4

List of Figures 7

List of Tables 9

List of Acronyms 10

Popular Science summary 12

1 Introduction 13

1.1 Trends in Wireless Communications 13

1.2 Purpose 14

1.3 Contribution 15

1.4 Organization 15

2 Background 17

2.1 In-Band Full-Duplex 18

2.2 Self-interference 19

2.2.1 Linear Component 19

2.2.2 Non-Linear Component 21

2.3 Analog and Digital Self-Interference Cancellation 22

2.3.1 Analog Self-Interference Cancellation 24

2.3.1.1 Passive Part 24

2.3.1.2 Active Part 25

2.3.2 Digital Self-Interference Cancellation 26

2.4 Time Synchronization 27

2.4.1 Primary Synchronization Signal (PSS) 28

2.4.2 Time Alignment 29

3 Proposed Time Synchronization Method 31

3.1 Primary Synchronization Signals 32

3.2 Cross-Correlation 33

3.3 Normalized Synchronization Peak (NSP) Detection and Time Synchronization Peak Index Switching 34

4 Performance Evaluation 37

4.1 System Specification 37

4.2 Simulator Description 38

4.2.1 Full-Duplex Transmission 38

4.2.1.1 Data Samples 38

4.2.1.2 Symbol Modulation Mapper 38

4.2.1.3 Zero Padding 39

4.2.1.4 Inverse Fast Fourier Transform IFFT 40

4.2.1.5 Cyclic Prefix Addition 40

4.2.1.6 Convolution 41

4.2.2 Full-Duplex Reception 41

4.2.2.1 Remove Cyclic Prefix and Channel Taps 41

4.2.2.2 Fast Fourier Transform FFT 41

4.2.2.3 Self-Interference Cancelation 42

4.2.2.4 Channel Equalization 42

4.2.2.5 Information Samples Extraction 43

4.2.2.6 Demodulation 43

4.3 Simulation Results 45

4.3.1 Synchronization Peak 45

4.3.2 Successful Synchronization Probability (SSP) 45

4.3.3 Peak detection Probability 47

5 Conclusion and Future work 53

References 54

List of Figures

Fig. 2.1. Half-duplex mode. 18

Fig. 2.2. In-band Full-duplex mode. 19

Fig. 2.3. Self-Interference in Full-Duplex communication. 20

Fig. 2.4. Two tones transmission in ideal (left) and real (right). 22

Fig. 2.5. Overview of the full-duplex and self-interference cancellation procedure. 23

Fig. 2.6. Self-cancellation budget. 26

Fig. 2.7. Synchronization affects SI cancellation. 27

Fig. 2.8. The correlation of primary synchronization signal. 28

Fig. 2.9. LTE uplink time-alignment [3]. 29

Fig. 2.10. Synchronization via time alignment. 29

Fig. 3.1. Half frame structure according to LTE standards, N_c is the number of samples in the timing estimate and the red highlighted slot is the location of the PSS signal. 31

Fig. 3.2. The zero padded PSS signal, null samples are placed on the edge of the band, and the PSS symbols are placed around the DC carrier. 33

Fig. 3.3. Theoretical success probability performance of full duplex timing. 36

Fig. 4.1. Desired Signal NSP (with root Index 25) peak value and Self-Interference NSP (with root Index 29) peak value depending on the channel quality. 45

Fig. 4.2. Successful synchronization probability performance of full-duplex synchronization according to NSP based desired and self-interference

signals.....49

Fig. 4.3. Full-Duplex BER Performance 50

Fig. 4.4. Full-Duplex BER Performance with the effect of the self-interference signal. 51

List of Tables

Table 4.1. System parameters.....37

Table 4.2. The percentage of the calculated cross-correlation maximum peaks at the correct sample index (15360).....46

Table 4.3. The average NSP corresponding to the desired and self-interference signal of the result values at the 20% access trial and the 25% access trial, according to the SNR in case 1 46

Table 4.4. The average NSP corresponding to the desired and self-interference signal of the resulting values at 20% access trial and 25% access trial, according to the SNR in case 2 47

Table 4.5. The average NSP corresponding to the desired and self-interference signal of the resulting values at 20% access trial and 25% access trial, according to the SNR in case 3 47

Table 4.6. The NSP based synchronization probability for the desired signal and desired threshold value α_th^((1))=8.9 at the desired SNR range 0, 10, 20, 30, and 40 dB.....48

Table 4.7. The NSP based synchronization probability for the self-interference signal and self-interference threshold value α_th^((2))=20 at the desired SNR range 0, 10, 20, 30, and 40 dB.....48

List of Acronyms

OFDM	Orthogonal Frequency Division Multiplexing
LTE	Long Term Evolution
PSS	Primary Synchronization Signal
4G/5G	4th /5th Generation
FDD/TDD	Frequency Division Duplex/Time Division Duplex
IBFD	In-Band Full-Duplex
MIMO	Multiple-Input and Multiple-Output
NR	New Radio
Mm-Wave	Millimeter-Wave
UE	User Equipment
BS	Base Station
IMS	IP Multimedia Core Subsystem
Tx /Rx	Transmitter/Receiver antenna
PA/LNA	Power Amplifier/Low Noise Amplifier
CP	Cyclic Prefix
SIC	Self-Interference Cancellation
IFFT/FFT	Inverse Fast Fourier Transform/ Fast Fourier Transform
DAC/ADC	Digital to Analog Converter/Analog to Digital Converter
PCB	Printed Circuit Board

SI	Self-Interference
SNR	Signal to Noise Ratio
ZC	Zadoff-Chu
QPSK	Quadrature Phase Shift Keying
NSP	Normalized Synchronization Peak
SSP	Successful Synchronization Probability
ISI	Intersymbol Interference
ICI	Intercarrier Interference

Popular Science summary

In-band full-duplex communication technology has gained high interest in the development of the current and next-generation wireless communication systems like the Internet of things (IoT) and the 5th generation network (5G). In-band full-duplex technology aims to absorb the remarkable increase of the network utilizers by tremendously increasing the data rate and the spectral efficiency. According to web reports, the amount of people who use the internet are 4.4 billion users out of 7.676B total population. The amount of the internet users has surged over the years, the analysis shows that there are more than one million new internet users since 2018.

In-band full-duplex serves as an attractive solution to overcome the problem of spectrum crunch, with twice the spectrum efficiency and having the potential to remarkably enhance the throughput of wireless communication systems as compared to the conventional, half-duplex communication systems. One of the key elements in full-duplex systems is the process known as “time synchronization in digital domain”. This technique helps to overcome a significant barrier in the operation of full-duplex systems, known as “self-interference”. Time synchronization in digital domain helps to cancel the self-interference and serves as a very effective solution.

This thesis aims to present a time synchronization technique for Orthogonal Frequency Division Multiplexing (OFDM) full-duplex transceiver based on Long Term Evolution (LTE). The performance of this technique is validated by a MATLAB simulation. In this method, time offset information is acquired for both the desired and the self-interference signals within a full-duplex node in order to improve the success rate of the synchronization probability. In order to achieve this, a Zadoff-Chu sequence is used with a different root index is utilized for the Primary Synchronization Signal (PSS)on each node. In addition, the adaptive cross-correlation peak detection of two kinds of PSSs in a full-duplex node, with the application of different threshold values is discussed.

CHAPTER 1

1 Introduction

In this chapter, the background of this thesis will be introduced. In the first subchapter, the main features and trends of conventional and new generation wireless communications are presented. The next subchapter describes the purpose of this thesis. Finally, a comparison between different traditional and novel techniques is presented along with the purpose and aim of this thesis.

1.1 Trends in Wireless Communications

Fourth Generation (4G) Long Term Evolution (LTE) has supported 100 Mbits/s data rate of the wireless device. It needs to share the network resources to support more simultaneous connection on the cell [1] [2]. 4G system is designed to support packet-data rather than circuit-switched voice. As it has been developed from release 8 to release 14, the peak data rates have grown to multi-Gbits/s nowadays [3]. During the process of 4G evolution, several technological advancements emerged to support their development, for example, Multiple-Input and Multiple-Output (MIMO) and Orthogonal frequency-division Multiplexing (OFDM). Furthermore, these technologies have been enhanced and will be applied for the use in 5G technology.

1. OFDM: OFDM is a modulation method based on frequency-division multiplexing. It splits a high data rate stream into a lot of low data rate, orthogonal and parallel subcarriers [4]. Thereby, the utilization of the frequency spectrum can be raised. By its character of the multi slow stream over a single carrier, OFDM can improve the propagation attenuation of high frequency, narrowband interference and frequency/selective fading by multipath transmission.
2. MIMO: This system is based on the multiple-element antennas system. Multiple-antenna system has been applied on both transmission and receiving ends instead of the conventional single antenna system. In this way, stronger signal can be achieved along with other upsides [4]. This

technology can integrate multiple radio capacity by a number of transmitting and receiving antennas. It has been applied in WiFi and LTE, and also, there are some smart antenna technologies are developed by MIMO, such as beamforming and diversity.

The tremendous increase in mobile traffic requires wireless solutions to provide higher data rates. In the past few years, researchers have been working on the development of next generation wireless communication systems, so-called 5th generation (5G) new radio (NR). For this purpose, they have been striving to accomplish key requirements to increase spectral efficiency and data rates. Some promising technologies have been introduced to address the improvement of spectral efficiency such as Massive MIMO, millimeter-wave (mm-Wave) communication and in-band full-duplex radios [5] [6] [7] [8]. The key features of the emerging technologies are as follows.

1. Mm-Wave communication: It means extremely high frequency band. It causes a high data rate and shorter wavelength, but larger distortion for long distance. The extremely high frequency band is defined as band frequency from 30 to 300 GHz. Therefore, the wavelength of mm-Wave is from 1 to 10 millimeter. When the wireless communication with mm-Wave, both the smaller frequency reuse distance and lower beamwidth of the antenna would be achieved.
2. Massive MIMO: based on the multi-user MIMO technology with a large number of antennas to increase capacity and coverage area. Therefore, the number of antennas should be increased in the array. These high-volume antennas array provide higher capacity, gain, adjustable beamforming to generate bigger coverage area.
3. In-Band Full-Duplex Radio (IBFD): The uplink and downlink transmissions exist in only one frequency spectrum. Besides, the User (UE) and Base Station (BS) can do transmission and receive at the same time. The utilization efficiency of expensive spectrum can be doubled. But the device will be affected by itself when it transmits to another device. Compare with traditional Listen-before-talk communication protocols to avoid signal collision, the In-Band Full-Duplex realize Listen-with-Talk without collision.

The common purpose of such technologies is to cope with much higher data rate requirements and a tremendous number of wireless connections. To achieve this, more efficient use of spectrum resource is imperative in common.

1.2 Purpose

This thesis focuses on IBFD as a key technology to make spectral efficiency higher. The key challenge of In-Band Full-Duplex faces is self-interference cancellation. And, successful synchronization is one of the most significant parts to

achieving more robust self-interference cancellation. Therefore, based on this motivation, we discuss a novel timing synchronization method of IBFD systems.

1.3 Contribution

In this thesis, we present a timing synchronization method for OFDM full-duplex transceiver based on LTE. Our contributions can be summarized as follows:

1. We systematically summarized the challenges of IBFD. Furthermore, we discuss the method to achieve a timing synchronization of IBFD. By doing that, we address the significance of synchronization in self-interference cancellation. This will be carried out in Chapter 2.
2. We present our timing synchronization of IBFD, which is based on two kinds of Normalized Synchronization Peak (NSP). By comparing the thresholds of NSPs, we discussed the criteria for evaluating the advancement of conventional and novel timing synchronization method. This will be carried out in Chapter 3.
3. Lastly, we evaluate our proposed method. To do this, the full-duplex simulator with LTE parameter was built by MATLAB. Our simulation results can be used to determine more reasonable verification standards for each of the 2 NSPs. These standards would lead to higher probabilities of successful synchronization, which would lead to more accurate self-interference cancellation. These simulation results and data would build a foundation for further exploration of the development of wireless communications. This will be carried out in Chapter 4 and Chapter 5.

1.4 Organization

The thesis is organized by:

In chapter 2, the background of technologies this thesis encounters and basic theory of IBFD are introduced.

In chapter 3, the purposed method for timing synchronization of IBFD is presented.

In chapter 4, the simulation results by MATLAB are provided.

In chapter 5, our thesis is concluded with future directions.

CHAPTER 2

2 Background

The telecom companies have been endeavored to improve the telecommunication technologies which can cope with the higher data stream. The entire industry has been focusing on this goal in the past years. The reason for such situation is getting an edge on the technology development would directly result in taking a lead in the volume of users. Mobile data traffic has been increased at a monthly rate of 88% during the year which from the fourth quarter of 2017 to the fourth quarter of 2018. The growth was 15 times larger than the growth in 2013. As a result, the volume of worldwide wireless communication subscriber has increased to 43 million. The total number of subscribers reached 7.9 billion by the fourth quarter of 2018 worldwide. [9].

Compare to the tremendous growth on the volume of subscriber and traffic stream, the frequency spectrum that can be utilized to accommodate the traffic stream in the wireless communication is a limited resource therefore hard to expand. Addition to that, various government and private sectors have been allocating their use of radio frequencies into a broader spectrum. This has also worsened the shortage of usable frequency spectrum in wireless communication. Above predicament has been defined as “Spectrum crunch”. The predicament has become the most essential technical obstacle to deal with the growing volume of the data stream. Therefore, the resolution of the predicament is the most important target of current wireless communication development.

By the end of 2017, the world’s first 5G NR solution was established with the purpose of resolving the Spectrum Crunch problem. And the mm-Wave communication is applied as one of the key technology for 5G NR. The character of mm-Wave, which the spectrum frequency is as broad as 30-300 GHz, makes it the perfect solution of Spectrum Crunch from technology aspect. However, the cost to obtain the license of commercially use of mm-Wave spectrum frequency is extremely high. For instance, a license for 1.8 GHz band was sold for over 40 billion USD in the US governmental auction in 2015 [10]. Since there is no way around the high cost to use the mm-Wave spectrum in wireless communication, the instant

improvement of the spectrum efficiency is necessary in order to lower the communication cost. Under such circumstances, IBFD is one of the alternatives to overcome the spectrum crunch. By using this technology, the same spectrum can now transmit twice the data stream as before in theory. In other word, the efficiency of the spectrum can increase up to 2 times by using the IBFD technology.

2.1 In-Band Full-Duplex

In 4G-LTE, half-duplex technologies frequency division duplex (FDD) and time division duplex (TDD) is widely used. The FDD means the data transmission from the UEs to base-station, which commonly called as uplink, and the data transmission from the base-station to UEs, which commonly called as downlink, is happened in the same time periods, but using the different carrier frequencies. On the contrary, The TDD means the uplink and downlink are carried out by the same carrier frequency but in time slots. The basic concept of FDD and TDD is shown in Fig 2.1.

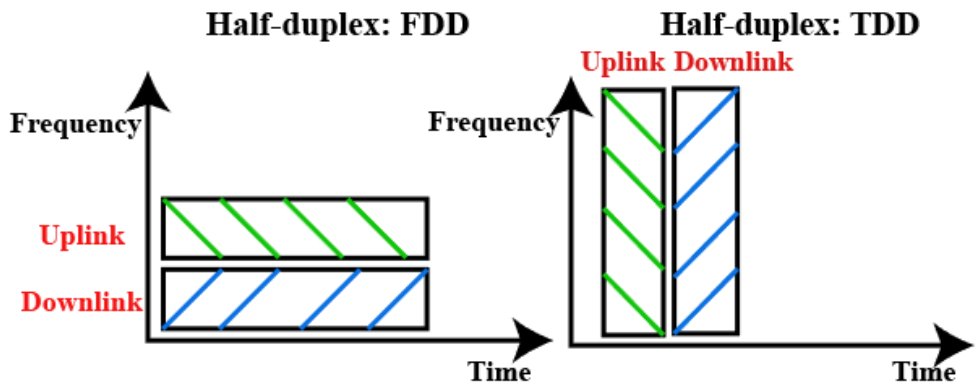

Fig. 2.1. Half-duplex mode.

However, as introduced above, both FDD and TDD have a major shortcoming which is the relatively low efficiency in the use of frequency spectrum. The researches were focused on considerably improve such efficiency. Early in 1997, G.R. Kenworthy has designed the first co-time co-frequency full-duplex system that can actually work since he integrated the patented “Self-cancelling Full-Duplex RF Communication System” [11]. The system creatively combines the radio frequency interference suppression technology and digital interference suppression technology to achieve better self-interference cancellation. The successful self-interference cancellation design has enlightened the possibility of upgrading FDD and TDD to co-time co-frequency full-duplex system, so-called In-Band Full-duplex. Since then, the better use of co-time co-frequency full-duplex system has become the theoretical starting point and research focus of frequency spectrum usage efficiency improvement.

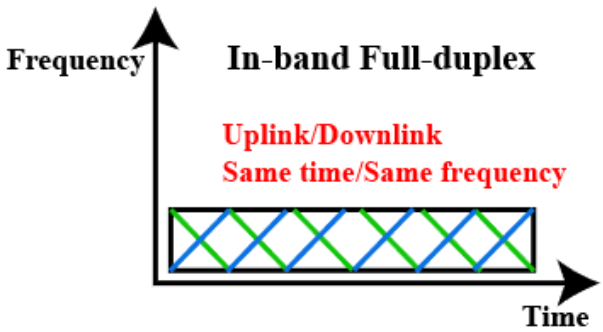

Fig. 2.2. In-band Full-duplex mode.

Compare to FDD and TDD, IBFD system provides the solution to mitigate the problem of Spectrum Crunch. The transceiver can receive and transmit data on the same frequency band at the same channel [12], as shown in Fig 2.2. However, the simultaneously uplink and downlink at the same channel also creates a problem of self-interference. The self-interference has limited the application of IBFD for a long time. In another word, IBFD can only be utilized when a successful and efficient self-interference cancellation is achieved.

2.2 Self-interference

The key challenge faced in in-band full-duplex systems is the strong self-interference signal imposed by one transceiver's transmit antenna onto its receiver antenna. For example, the data sent by transceiver A is also received by itself. Therefore, this signal becomes noise to the desired signal which is sent by transceiver B. This process is called Self-interference [13].

In cellular and WiFi systems, the transmit power can reach up to 20 dBm and the typical receiver noise floor is -90 dBm with a bandwidth of 20 MHz [14]. Therefore, around 110 dB of self-interference noise cancellation is needed to decide the desired signal. If the self-interference is not canceled up to noise floor, it affects the desired signal as a strong interference.

In this subchapter, the self-interference (SI) will be introduced in detail. This part presents what is the SI and where is it from. In the later, the SI will be written by 2 components: linear and non-linear components.

2.2.1 Linear Component

Depending on some specific characteristics of the full-duplex system, for instance, the specifications of the RF circuit components or the number of antennas been used, several components of SI can be recognized. Simplify speaking, linearity can be used as the criteria to distinguishing different components. The linear component often refers to the overlap of the delayed, attenuated and original desired

signal between the transmit and receive antennas. In a single-antenna system, such delay and attenuation can be caused by distance, obstacles, leakage of a circulator or simply reflection, etc. Delays and attenuators, as component of RF circuit, are often be used to simulate the linear component for analog self-interference canceller (SIC). The delays and attenuators are frequently used for the purpose of channel estimation, as in most conventional wireless communication systems [15].

A wireless link is easier to illustrate with a linear system. Under the assumption, transmitted signal always goes through a linear system when it was transmitted from a digital-to-analog converter (DAC) to analog-to-digital converter (ADC). The content of the received signal can be illustrated as follow: [15]

$$y[n] = h[0]s[n] + h[1]s[n - 1] + \cdots + h[L]s[n - L] + z[n] \qquad (2.1)$$

In which $y[n]$ is received signal. In the (2.1), n represents the time index, while h represents the propagation which is actually the linear coefficients. L is the longest delay spread of the channel. And $s[n]$ and $z[n]$ are, respectively, the transmitted signal and noise.

The red line in Fig 2.3 represents a linear system of SI. As shown in Fig 2.3, the existence of the linear component of self-interference arises the problem that self-generated signal could interfere with the desired signal on its receiving antenna, therefore degraded the desired signal.

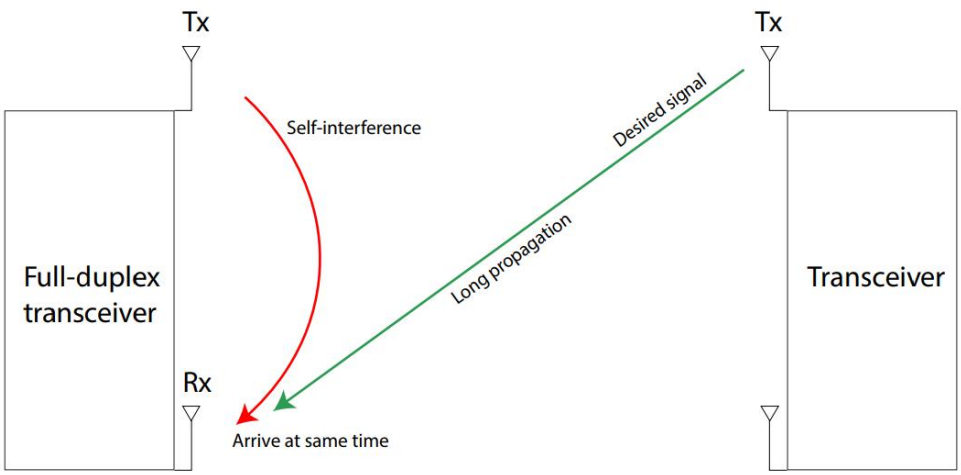

Fig. 2.3. Self-Interference in Full-Duplex communication.

Practically, the propagation distance of the desired signal is longer than the self-interference signal in most of the cases. Propagation attenuation caused by this longer distance results in transceiver receiving stronger self-interference signal than

the desired signal. For the purpose of extracting accurate desired signal, self-interference signal has to be correctly recognized. Only in that case self-interference signal can be canceled out [4].

In most of the cases, the power of the self-interference signal is around 20 dBm and vary from 18 dBm to 23 dBm. On the other hand, the ambient noise floor of transceiver is around -90 dBm. Therefore in this thesis, for the purpose of controlling variables and making the discussion feasible, we assume the power of self-interference signal is 20 dBm and the power of noise floor is -90 dBm. The gap between these two is 110 dB which says we assume the power of linear self-interference is 110 dB [12] [16].

2.2.2 Non-Linear Component

In the ideal situation, the transmitted signals can be directly created. However, there are no perfect circuits and electronics existed in the real world. Non-Linear components are usually generated by non-ideal circuits components, such as power amplifiers (PA) in transmitters and low-noise amplifiers (LNA) in receivers. High order nonlinearity of the power amplifier is easily generated from the high peak-to-average ratio signal which comes from OFDM or wideband code division multiple access. This is because the high-power input signal offset the power of the output signal.

The nonlinearity interferes with linear SI. To estimate the intermodulation distortion which is caused by nonlinearity, a Taylor series is usually used. Because the even-ordered terms are out of the band. Therefore, only odd-ordered terms remain in the Taylor series [15]. The input signal x will be exported with non-linear cubic and higher odd-ordered terms, such as x3, x5 or higher [15] [17] [18] [19]. Such an output signal of the amplifier, y(t) can be represented as: [20]

$$y(t) = \sum_{i=1}^{\infty} a_{2i+1} x^{2i+1}(t) \tag{2.2}$$

In which *x(t)* is the input signal in continuous time *t* and *a* is the non-linear coefficient, also, *2i+1* component represents the (2i+1)th of the power series representation.

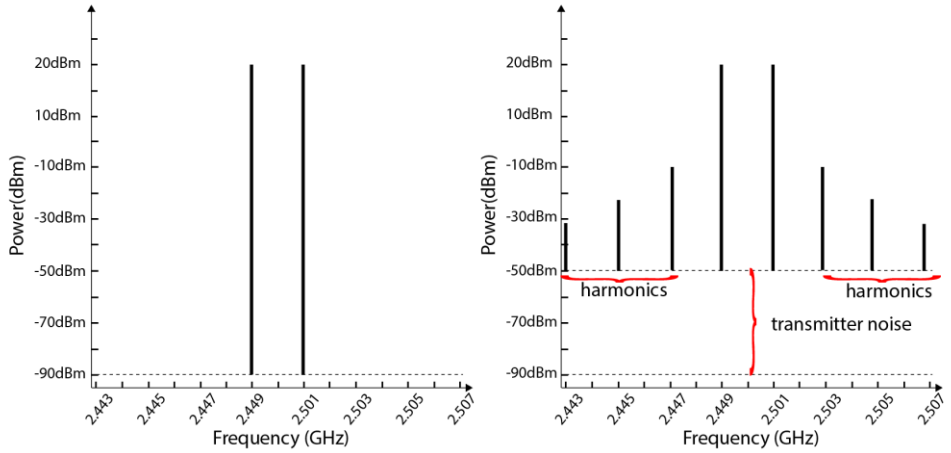

Fig. 2.4. Two tones transmission in ideal (left) and real (right).

From the above Fig 2.4, the non-linear components are precisely illustrated. Assume that there is a 1 MHz sine wave signal transmitted with 2.45 GHz carry frequency. The power of this sine wave is 20 dBm. Without any other factor, this causes that two tones are generated in 1MHz away from 2.45GHz. these two tones have been shown in the left of Figure as 2 black straight lines on the 2.449 GHz and 2.451 GHz.

From the practical part (right chart) of Fig 2.4, six more symmetrical black lines appear on both sides of the original 2 tones. They can be collectively called as harmonics or so-called non-linear noise. By the property of harmonic, they will local at double, triple and so on integer multiple of the reference frequency. By this assume, the reference frequencies are 1 MHz away from 2.45 GHz (original two tones). Then, the harmonics local at 2.443, 2.445, 2.447, 2.503, 2.505, 2.507 GHz by the limited displayed frequency domain in the right of figure. By the researching, the power of harmonics will reach to -10 dBm. [12] Which means, there are at least 80 dB non-linear noise should be canceled by self-interference cancellation.

In the following chapters, our discussion will be focused only on the cancellation of 110 dB of linear SI. This is because that non-linear SI is completely canceled by the hardware in the receivers in the conventional technologies. For instance, when there is a 14-bit ADC in the receiver, a total of 86.04 dB which is calculated by (6.02 *14+1.76) dB [15] of non-linear SI can be canceled. In the calculation, the 14 is the number of bits of the ADC.

2.3 Analog and Digital Self-Interference Cancellation

Fig 2.5 is an illustration of the overall structure of the full-duplex system. The self-interference cancellation mechanism has also been marked. The self-interference cancellation architecture consists of spatial isolation, digital self-

interference canceller (SIC) and analog SIC. Among them, spatial isolation and analog SIC are SI cancellation in the analog domain while digital SIC is SI cancellation in digital domain.

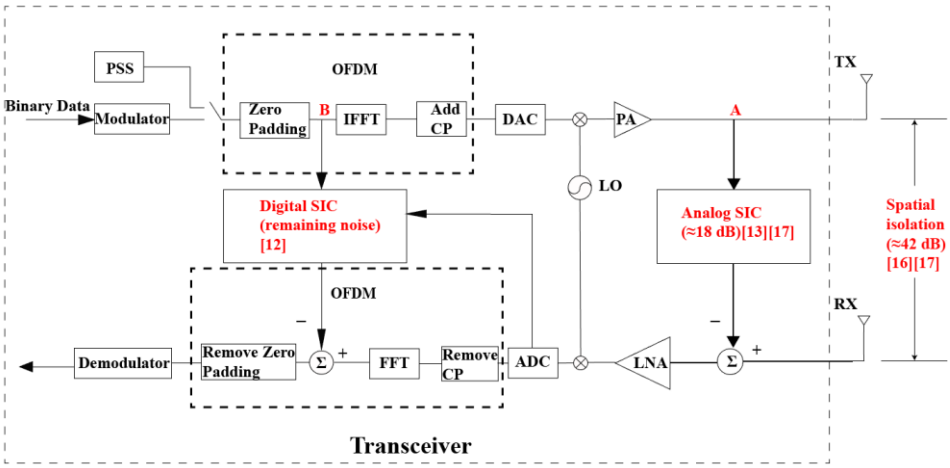

Fig. 2.5. Overview of the full-duplex and self-interference cancellation procedure.

In a full-duplex transmitter chain, the binary data goes through the modulator and outputs the modulated symbols. The PSS will be inserted into these symbols in specific positions. Then, the signals go through OFDM, DAC and PA modules. From this point on, the signal is ready to be transmitted. In the transceiver, the receiving chain includes similar modules but in reverse sequence comparing to transmitting chain, if self-interference cancellation modules are not taking into consideration. When the transmitted signal reaches the receiver chain, the desired and self-interference signals will be obtained by RX. Then, the signals experience the reverse process of the transmitter chain.

In the analog self-interference cancellation, it can be divided into passive cancellation and active cancellation. The passive cancellation corresponds to spatial isolation. This isolation effect can be achieved by the adjustment of distance, material and polarization of antennas. The active cancellation can be achieved by Analog SIC sending a same but delayed analog signal to neutralize self-interference signal in the analog domain. The analog canceller is most effective at handling strong signals with a short delay spread before the Low Noise Amplifier (LNA) and Analog-to-Digital Converter (ADC) in the analog domain [21].

The digital SI cancellation method is different from the one used in the analog domain. It is achieved by Digital SIC sending a same but delayed and destroyed digital signal to neutralize SI signal in the digital domain. The use of digital SIC is most effective at handling weak signals with delays greater than 1,000 nanoseconds after ADC and Fast Fourier Transform (FFT) in the digital domain [22] [23].

The cancellation process sequences will be discussed in detail in the upcoming chapter.

2.3.1 Analog Self-Interference Cancellation

In the analog domain, self-interference (SI) in a full-duplex system can be carried out through passive and active methods. The passive part is demonstrated in Fig 2.5 as spatial isolation and active part is shown as Analog SIC process. With spatial isolation, at least 42 dB SI can be canceled. And by analog SIC active process, 18 dB SI can be cancelled [17] [24] [25] [26].

2.3.1.1 Passive Part

Spatial isolation is generally a passive, analog way to reduce the transmitter power as interference for the receiver. Usually, spatial isolation can be processed by three methods:

1. Circulator: circulator is a passive 3-port device. And it is suitable as an isolation part of a single antenna IBFD system. For example, in a circulator, port one is connected to a transmitting chain, port two is connected to an antenna, and port three is connected to the receiving chain. When the transmitting signal passed through port 1 and reached port 2, the circulator act as an isolator between port 2 and port 3. Therefore, the signal will not be transmitted to port 3. Such a circulator could provide up to 15-20 dB isolation [15] [17].
2. Distance Isolation: After electromagnetic signals have been sent out, these signals will experience path loss. The idea in distance isolation is to separate TX and RX as far away as possible, without affecting transmission efficiency, and then the signal power will be reduced exponentially. Through experiment results, 50 dB SI can be reduced if the TX and RX can be divided by 40 cm [17].
3. Polarization Isolation: Both TX and RX have their own best direction of transmitting or receiving signal. To avoid the intervene between the polarization direction of TX and RX would result in better signal transmission. For example, in a dual-polarization antenna, TX and RX are integrated on one printed circuit board (PCB). The polarization directions of TX and RX are orthogonal. Therefore, passive and simple isolation is achieved.

In 5G systems, there would be no enough space to separate the TX and RX. Addition to that, IBFD in 5G system needs multi-antenna to achieve co-time co-frequency transceiving function. In that case, a highly integrated antenna known as a dual-polarization antenna was developed to achieve polarization isolation. According to experimental data, using these techniques, 42 dB of self-interference signals can be canceled [16] [17].

2.3.1.2 Active Part

An around 18 dB SI was canceled by applying an "Analog SI canceller" technique in analog domain [12] [27]. It has been shown in Fig 2.5 as analog SIC from node A. From the auxiliary chain by node A, the complete copy of the analog transmit signal will be carried to the analog SIC. Then, the function of analog SIC is to simulate the channel between TX and RX and generate estimated SI for cancellation in the analog domain [28]. This process can be represented in mathematical form as:

$$y[t] = h[n] * s_d[n] + g[n] * s_{si}[n] + z[n] \tag{2.3}$$

Equation (2.3) explains the components of the signal received by the transceiver $y[n]$ in the time domain, and the n is the time index. $s_d[n]$ represents the desired signal. And $h[n]$ represents the channel which desired signal experienced in the time domain. The symbol * represents the convolution process.

The second component $g[n] * s_{si}[n]$ represents SI signal which has experienced its own channel. $s_{si}[n]$ indicates the original SI signal generated by transceiver and $g[n]$ indicates the self-interference channel over time n.

Finally, $z[n]$ is thermal noise in the receiver.

$$\hat{e}_A[n] = \hat{g}_A[n] * s_{si}[n] \tag{2.4}$$

Equation (2.4), the $\hat{e}_A[n]$ represents the estimated SI signal which is outputted by analog SIC in Fig 2.5. The $\hat{g}_A[n]$ is the estimated channel experienced by SI and the $s_{si}[n]$ represents the SI signal from node A in Fig 2.5.

$$\begin{aligned} y_A[n] &= y[n] - \hat{e}_A[n] \\ &= h[n] * s_d[n] + (g[n] * s_{si}[n] - \hat{g}_A[n] * s_{si}[n]) + z[n] \\ &= h[n] * s_d[n] + z_{si}[n] + z[n] \end{aligned} \tag{2.5}$$

The $y_A[n]$ represents the signal left after the neutralization of estimated SI from the received signal before LNA in receiving chain. The $z_{si}[n]$ represents the residual interference after SI cancellation. There are 18 dB of SI can be removed by this active analog self-interference cancellation [13] [17].

Overall, a total of 60 dB (42 dB by passive part and 18 dB by active part) of self-interference can be solved in the analog domain. In the previous discussion, we have set the total SI at 110 dB. Therefore, around 50 dB of SI remains. These SI have to be canceled in the digital domain.

2.3.2 Digital Self-Interference Cancellation

As explained earlier, there are 60 dB self-interference can be removed through the analog domain. Assuming that the level of self-interference is 110 dB and there is a total of 60 dB that has been suppressed at all noise components by polarization isolation and analog SI canceller [12]. For this reason, Fig 2.6 represents that 50 dB SI should still be observed in the receiver [28].

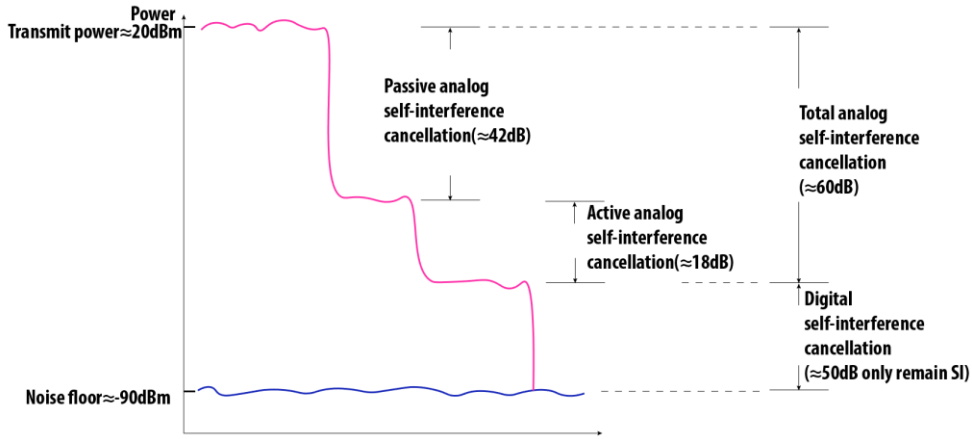

Fig. 2.6. Self-cancellation budget.

The operation mechanism of digital SIC is similar to analog SIC: they both use the estimated channel to generate an antipodal estimated SI signal in order to neutralize the SI signal. The difference between digital SIC and analog SIC is mainly the domain of the estimated channel and the signal resource which used to generate the estimated channel. In the digital SIC block, it takes the digital transmitted signal and residue SI signal which have processed by analog SIC to generate estimated channel. Detailed speaking, received signal is first converted by ADC and FFT after analog SI cancellation. After that, it enters into the digital domain in order to perform channel estimation meanwhile neutralize the remaining of the SI signal.

The demonstration of such neutralization is similar to (2.3) to (2.5) above [28]. Similar to (2.5), the signal left after digital SI cancellation are calculated as below:

$$\begin{aligned}\hat{Y}[k] &= y_A[k] - \hat{e}_D[k] \\ &= h[k] * s_d[k] + z_{si}[k] + z[k] - \hat{g}_D[k] s_{si}[k]\end{aligned} \tag{2.6}$$

The $y_A[k]$ represents the received signal after analog SIC as which has been calculated in (2.3) but appearing as the digital domain. So the $h[k] * s_d[k]$, $z_{si}[k]$ and $z[k]$ represent the desired signals which have experienced channel, remaining SI after Analog SIC, thermal noise, respectively, all in Digital domain out of (2.5).

And the k represents the frequency index, the size of k depends on the size of IFFT/FFT.

Also, the $\hat{e}_D[k] = \hat{g}_D[k]s_{si}[k]$ means the estimated SI signals. It consists of the estimated channel in the frequency domain from Digital SIC $\hat{g}_D[k]$ and original SI signals from node B $s_{si}[k]$. Therefore, (2.6) can be rewritten as:

$$\begin{aligned}\hat{Y}[k] &= h[k] * s_d[k] + (z_{si}[k] - \hat{g}_D[k]s_{si}[k]) + z[k] \\ &= h[k] * s_d[k] + \hat{z}_{si}[k] + z[k]\end{aligned} \tag{2.7}$$

Here the $\hat{z}_{si}[k]$ represents the remaining noise after Analog and Digital SIC.

According to research experiments result, around 84 dB linear can further be solved in digital domain [12]. Hereto, the generated SI signal in which a total of 110 dB linear and 80 dB non-linear can be cancelled theoretically. However, in the practical scenario, there is still a small residual SI remained in the transceiver due to the fact that the transceiver cannot estimate the channel perfectly every time.

2.4 Time Synchronization

Time synchronization plays a crucial part in SI cancellation. The accurate time synchronization is the foundation of SI cancellation. This thesis is focusing on time synchronization and proposed a way to achieve better time synchronization.

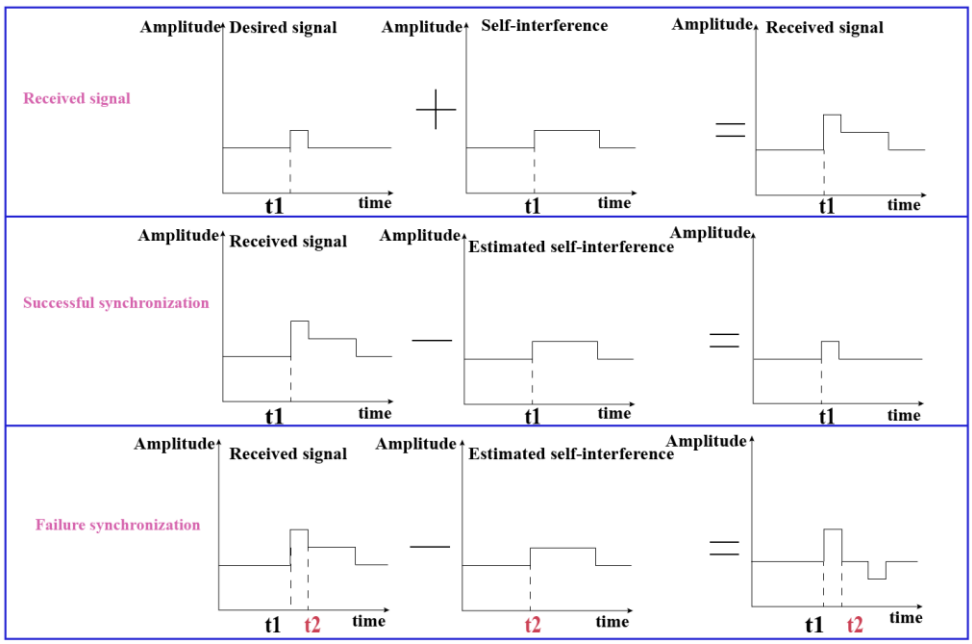

Fig. 2.7. Synchronization affects SI cancellation.

Fig 2.7 explains the importance of synchronization for SI cancellation. The first row of equation shows that the received signal is an accumulation of the desired and SI signals. The second row shows that SI can be neutralized with estimated SI under successful time synchronization. The third row presents the distortion of the received signal compared to the original signal under a failure time synchronization. The t2 in the third figure equation represents the starting point of time for estimated SI when there is a failure in time synchronization. From the illustration, the importance of successful time synchronization in the SI cancellation becomes obvious [29] [30].

To achieve a successful time synchronization, the correct use of two key technologies, namely Primary Synchronization Signal (PSS) and time alignment, are expected.

2.4.1 Primary Synchronization Signal (PSS)

PSS is used in synchronization processing for the detection of the signal starting point.

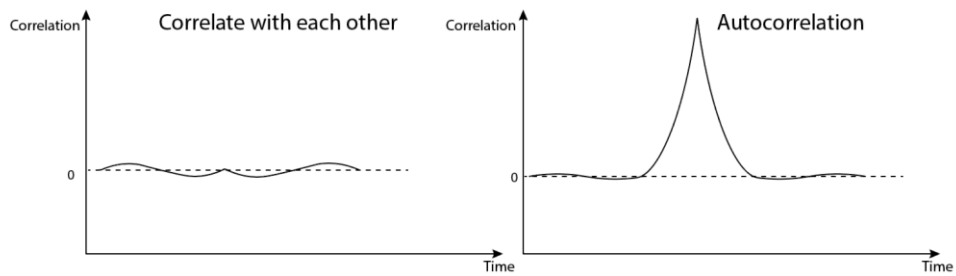

Fig. 2.8. The correlation of primary synchronization signal.

For PSS signals, the correlation is represented in Fig 2.8. The correlation can be illustrated by the similarity between the two signals. So, the example on the left shows that there are no peaks created by the two signals, and the right part will show highly similar degree if these two signals are the same [29]. So, the synchronization of SI and the desired signal can be separately detected if they apply individual PSS.

2.4.2 Time Alignment

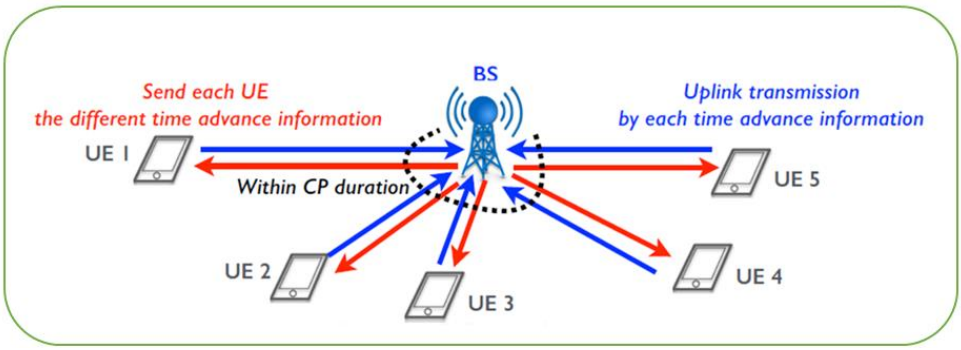

Fig. 2.9. LTE uplink time-alignment [3].

Time alignment is used in the uplink process of conventional cellular systems. As shown in the above diagram, UEs are regulated by BS. When the uplink signals are sent from UEs to BS, BS sends back timing advance control information for communication to every UE. The transmitting time is shared via control packets in order to regulate and maintain the time at which the data is sent by UE. Therefore, with the time alignment, data propagation delays of UEs can be counteracted provided that the signals fall within the length of an uplink cyclic prefix (CP) [31].

Fig. 2.10. Synchronization via time alignment.

In Fig 2.10, time alignment is adopted to suppress propagation delay between the self-interference signal and the desired signal. With the time alignment applied, the intra-cell interference and ISI can be solved through operations in the base stations, for instance, when the self-interference signal and the desired signal reach the length of CP over uplink, they can be seen as that they arrived at transceiver at same time [28].

Overall, successful time synchronization can be realized by applying the technologies of PSS and time alignment. In next chapter, a more advanced way of applying PSS will be introduced to achieve the purpose of this thesis: the application of synchronization peak switching in the time synchronization process, which could lead to the result of the higher probability of successful time synchronization. With this synchronization peak switching technology, 2 individual PSS will be allocated to transmitted and desired signals respectively. Therefore, the data source of time synchronization becomes both SI and desired signal.

CHAPTER 3

3 Proposed Time Synchronization Method

In full-duplex communication, it is crucial to have a synchronization protocol between the full-duplex transmitter and receiver. Hence, for stable performance for self-interference cancellation, a robust synchronization method is an essential requirement [16]. We consider a frame structure based on LTE downlink standard for both uplink and downlink transmission of full-duplex link as illustrated in Fig 3.1 [3]. Two half frames are modeled; one for the desired signal and the other for the self-interference signal. Each half frame is divided into five sub-frames, each sub-frame consist of 2 slots with equal size [3], each slot includes 6 OFDM symbols with 512 samples cyclic prefix length (LTE extended mode) [3]. Hence the half frame contains 60 OFDM symbols.

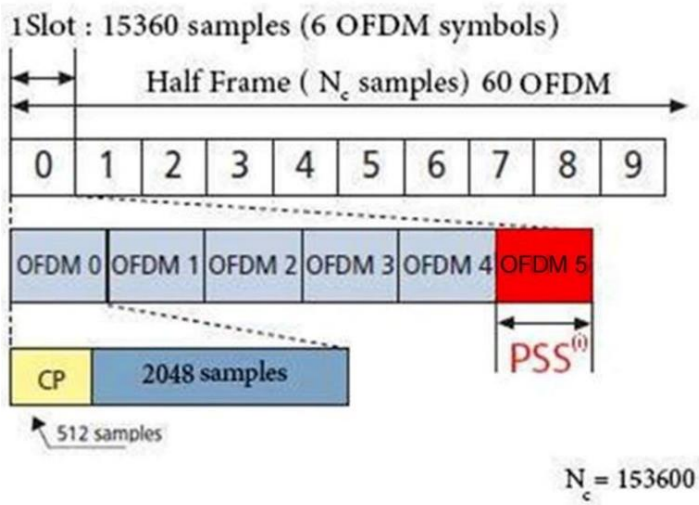

Fig. 3.1. Half frame structure according to LTE standards, N_c is the number of samples in the timing estimate and the red highlighted slot is the location of the PSS signal.

3.1 Primary Synchronization Signals

For timing synchronization, a PSS is constructed and transmitted [3]. The PSS is situated in the last OFDM symbol of the first slot in the half frame, as shown in the right side from Fig 3.1.

The length of the PSS is 62 Zadoff-Chu (ZC) sequence [28], it is modulated with a subcarrier index; k, around the DC-carrier. The ZC sequence is modulated as following:

$$P_{(i)}[k] = \begin{cases} e^{-j\frac{\pi u^{(i)}}{N_p}k(k+1)} & if\ -31 \leq k \leq -1 \\ e^{-j\frac{\pi u^{(i)}}{N_p}k(k+1)(k+2)} & if\ 1 \leq k \leq 31 \end{cases}, \quad (3.1)$$

Where $u^{(i)}$ is an element among the root indices defined in LTE standard [28], $N_p = 62$ [28]. Exploiting the special properties of ZC sequences:

1. The sequences have a constant amplitude, from 3.1, the parameter $e^{-j(\Theta)}$ is mathematically equal to $cos(\Theta) - j\ sin(\Theta)$ which result in a long sequence of complex numbers with an amplitude of 1, where all the sequence values lie on the border of a circle. [32].
2. Two ZC sequences with different root indices $u^{(1)}, u^{(2)}$ are orthogonal to each other [28], applying $u^{(1)} = 25$ for the desired PSS and $u^{(2)} = 29$ for the self-interference PSS (the values are based on LTE standards) [28].

Both $p_{(1)}$ and $p_{(2)}$ sequences for the desired signal and self-interference signal, with respect to the root index $u^{(i)}$, are zero-padded with FFT size, structured as 1985 nulls at the edges and sequenced with 62 ZC sequence around the DC carrier, as shown in Fig 3.2. As all the OFDM symbols are in the time domain at the transmitter stage, the $P_{(i)}$ is fed to the inverse fast Fourier transform (IFFT) block in order to convert it to the time domain. The IFFT process for the desired and self-interference p_i sequences are given as follows:

$$p^{(i)}[n] = \sum_{k=-\frac{N_p}{2}}^{\frac{N_p}{2}} P_i[k] e^{j\frac{2\pi}{N_{FFT}}kn} \quad (3.2)$$

Where $p^{(i)}$ represents the desired and self-interference PSS signals which are at IFFT points of a ZC sequence with respect to the root index $u^{(i)}$ and $n = 0,1,2,\dots,N_{FFT} - 1$, where N_{FFT} indicates the IFFT size. Like the IFFT process for the desired and self-interference signals, the length of the ZC sequence is less than the length of IFFT, so that the power of the $p^{(i)}$ must be normalized. The power of the PSS signals is scaled by the factor $\frac{N_{FFT}}{\sqrt{N_p}}$; Hence, the IFFT output $PSS^{(i)}$ is as given as [32]

$$PSS^{(i)}[\mathrm{t}] = \frac{N_{FFT}}{\sqrt{N_p}}\, p^{(i)} \tag{3.3}$$

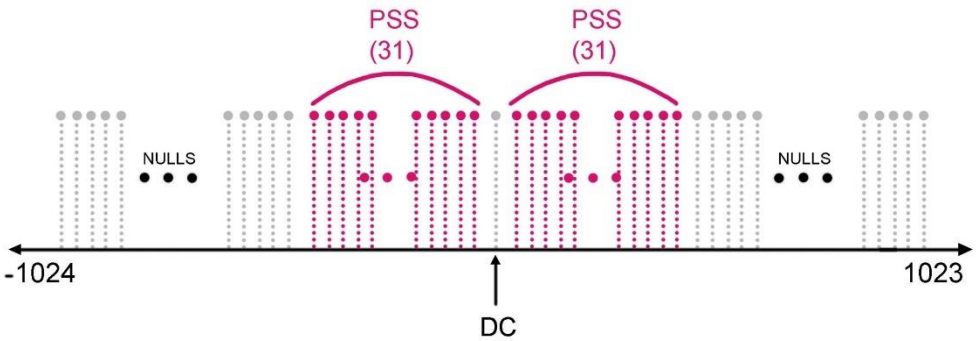

Fig. 3.2. The zero padded PSS signal, null samples are placed on the edge of the band, and the PSS symbols are placed around the DC carrier.

3.2 Cross-Correlation

Cross-correlation shows the similarity of two sequences as a function of the lag of one relative to the other [33]. The reason behind modulating two PSS signals with different ZC root indices ($u^{(1)}, u^{(2)}$) is for synchronization between the received and self-interference signals. The receiver detects the starting point of the OFDM symbol by measuring the index of the maximum value of cross-correlation of the received signals with the desired and self-interference $PSS^{(i)}$ (with respect to the root index $u^{(i)}$ after the IFFT process). This is mathematically denoted as:

$$C^{(i)}[\tau] = \left|\sum_{n=0}^{N_{FFT}-1} y[n+\tau] PSS^{(i)*}[n]\right| \tag{3.4}$$

$$n = 0,1,2,\ldots N_{FFT} - 1$$

And the maximum value of the cross-correlation is denoted as:

$$\Lambda^{(i)} = \arg max_{\tau}\ C^{(i)}[\tau] \tag{3.5}$$

Where $(.)^*$ denotes the complex conjugation, τ denotes the lag between the two sequences, and y is the received full-duplex signal that contains the noisy desired signal and self-interference signal. Therefore, a maximum peak is detected at the sample index of the first sample of the OFDM symbol following the $PSS^{(i)}$ symbol [13]. Furthermore, the starting indexes are also detected for the desired signal and for the self-interference signal.

3.3 Normalized Synchronization Peak (NSP) Detection and Time Synchronization Peak Index Switching

The NSP is defined as the ratio between the cross-correlation peak value and the average values of the cross-correlation [28], given as:

$$\alpha^{(i)} = \frac{C^{(i)}[\Lambda^{(i)}]}{\frac{1}{N_c}\sum_{d=0}^{N_c} C^{(i)}[\tau]} \tag{3.6}$$

Where $\alpha^{(i)}$ is the NSP value with respect to the root index $u^{(i)}$, and N_c is the total number of samples in the half frame (10 slots). The output value $\alpha^{(i)}$ with respect to the root index $u^{(i)}$ depends on the SNR for both the desired channel $\mathrm{SNR_d}$ and the self-interference channel $\mathrm{SNR_{si}}$.

The synchronization decision is taken by the optimization of two threshold values, $\alpha_{th}^{(i)}$ with respect to the root index $u^{(i)}$, e.g., $\alpha_{th}^{(1)}$ for the desired signal and $\alpha_{th}^{(2)}$ for the self-interference signal. Hence, a successful synchronization occurs in a scenario of NSP, where $\alpha^{(i)}$ values are bigger than $\alpha_{th}^{(i)}$. Successful synchronization probability is calculated considering the following variables:

1. Access trial number, defined as N_{trial}
2. Successful Detection: The event where $\alpha^{(i)}$ is bigger than $\alpha_{th}^{(i)}$, and the maximum value of the cross-correlation $\Lambda^{(i)}$ is decided as the correct index.

$$P_s^{u^{(i)}} = \mathrm{P}\left(\alpha^{(i)} > \alpha_{th}^{(i)}\right) \tag{3.7}$$

3. False alarm: In an event when $\alpha^{(i)}$ is successfully detected, but the maximum value of the cross-correlation $\Lambda^{(i)}$ is not considered as the correct index, this is referring to a false alarm.

$$P_F^{u^{(i)}} = P\left(\hat{d} = d_c \mid \alpha^{(i)} > \alpha_{th}^{(i)}\right) \tag{3.8}$$

Where $\hat{d}$ is the estimated index and d_c is the current index.

4. Not Detected: The event when $\alpha^{(i)}$ is smaller than $\alpha_{th}^{(i)}$,

$$P_{Not}^{u^{(i)}} = \mathrm{P}\left(\alpha^{(i)} < \alpha_{th}^{(i)}\right) \tag{3.9}$$

Hence the successful synchronization probability (SSP) is given as:

$$P_{ss}^{(i)} = \frac{P_s^{u^{(i)}}}{N_{trial} - P_{Not}^{u^{(i)}}} \tag{3.10}$$

Where $P_{ss}^{(i)}$ denotes the successful synchronization probability.

Therefore, for good probability performance, the event $P_{Not}^{u^{(i)}}$ is adjusted to reach a maximum probability of 25%. This is accomplished by using two threshold values, $\alpha_{th}^{(i)}$ with respect to the root index $u^{(i)}$, as the overall signal to noise ratio for the self-interference ($\mathrm{SNR_{SI}}$) is high, the self- interference $P_s^{u^{(2)}}$ will also be high at low signal to noise ratio for the desired signal ($\mathrm{SNR_d}$) level, while the desired $P_s^{u^{(1)}}$ is almost zero. When the $\mathrm{SNR_d}$ is high, $P_s^{u^{(1)}}$ is dominant. Therefore, $\alpha_{th}^{(i)}$ is measured by investigating the NSP $\alpha^{(i)}$ values during different $\mathrm{SNR_d}$ and the self-interference $\mathrm{SNR_{si}}$ powers, then sorting $\alpha^{(i)}$ values from the minimum to the maximum.

Hence at a high level $\mathrm{SNR_d}$ when $P_s^{u^{(1)}}$ reaches dominance, the desired threshold value $\alpha_{th}^{(1)}$ is optimized as the average values of $\alpha^{(1)}$ at the 20 % access trail and 25% access trial, after sorting $\alpha^{(1)}$ values from minimum to maximum so that the desired $P_{Not}^{u^{(1)}}$ does not exceed 20 to 25%. Likewise, when the $\mathrm{SNR_d}$ power is low, the self-interference $P_s^{u^{(2)}}$ becomes dominant, because the $\mathrm{SNR_{SI}}$ is much higher, which degrades the NSP $\alpha^{(2)}$ values. The self-interference $\alpha_{th}^{(2)}$ value is optimized as the average values of the result $\alpha^{(2)}$ at 20% and 25% access trial, after sorting $\alpha^{(2)}$ values from minimum to maximum in order that the self-interference $P_{Not}^{u^{(2)}}$ does not exceed 20 to 25 %.

Hence to detect the time offset between the desired and self-interference signals, in practical, the starting index of the desired signal is delivered into FFT operation, and the starting index of the self-interference signal is delivered for self-interference cancellation [13].

Then a successful timing synchronization with respect to root index is considered when the NSP $\alpha^{(i)}$ is bigger than $\alpha_{th}^{(i)}$.

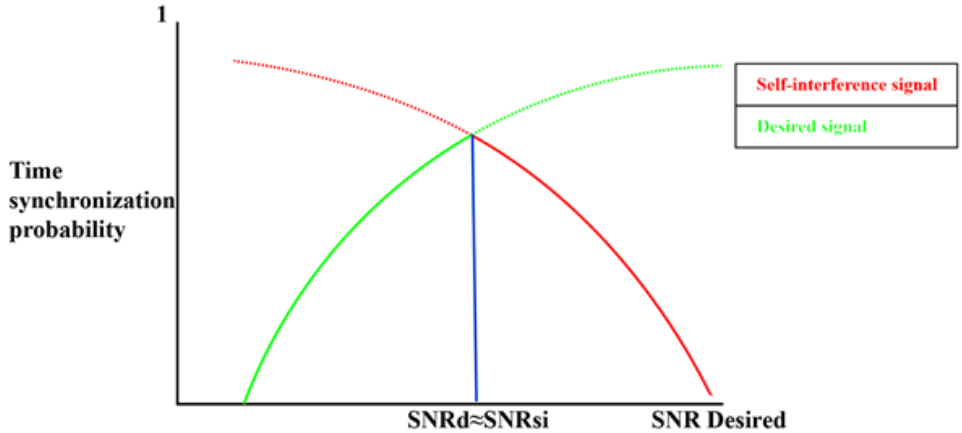

Fig. 3.3. Theoretical success probability performance of full duplex timing.

CHAPTER 4

4 Performance Evaluation

In this chapter, the simulation result of the proposed OFDM full-duplex transceiver is evaluated. The remainder of this chapter is structured into three parts; the first part provides the simulation parameters for performance evaluation, the second part describes the LTE-like full-duplex simulator, and finally, we illustrate the performance results of our proposed method.

4.1 System Specification

In this subchapter, we design a time synchronization method for orthogonal frequency division multiplexing (OFDM) full-duplex transceiver based on Long Term Evolution (LTE), and evaluate the system performance using MATLAB simulation. In the proposed method, we will acquire time offset information of both desired and self-interference signals in a full-duplex node, to enhance the successful synchronization probability. To achieve this, a Zadoff-Chu sequence with a different root index is used for the primary synchronization signal (PSS) at each node. The parameters for the OFDM full-duplex transceiver are defined and simulated based on long-term evolution (LTE) standards as the following [3]:

Table 4.1. System parameters

Parameter	Value
FFT size	2048
$\mathbf{N_{samples}}$	1200 (Per OFDM symbol)
$\mathbf{N_{cp}}$	512 (Extended CP in LTE)

4.2 Simulator Description

The desired signal is assumed to be transmitted from a partner user node with SNR range 0 to 40 dB, and the self-interference Signal is transmitted at the full-duplex node with fixed residual self-interference SNR power of 40dB.

4.2.1 Full-Duplex Transmission

4.2.1.1 Data Samples

The information sampler is the first principal step of the OFDM full-duplex transmitter. Serial information is generated for the desired bits and self-interference bits and fed as input in this step, which yields several desired and self-interference samples according to the modulation type and IQ (imaginary and quadrature) order [34]. Here, the output will be a group of desired and self-interference symbols, each containing the number of samples. This is to pre-form groups of bits (symbol) to be transmitted.

4.2.1.2 Symbol Modulation Mapper

The desired and self-interference symbols are equally mapped. The data is first converted from serial stream to parallel stream, contingent on the number of information samples. Since there are specified $Nsamples$ permitted for the OFDM transmission, the samples are then indexed as $(0,1,2,\dots,Nsamples-1)$. Serial to Parallel converter receives the serial stream of input bits and outputs $Nsamples$ parallel streams [35]. The performed symbols from the previous stage are fed as an input to the mapper to map the desired modulation scheme and order [34]. In this simulation, QPSK, 16-QAM, and 64-QAM modulation schemes are used. The symbols are generated concerning the constellation diagram.

$$K = log_2(M) \text{ Bits} \tag{4.1}$$

Where K represents the number of bits per symbol and M (4,16 and 64) is the modulation order.

Furthermore, the modulated desired symbols are denoted as $s_{d\_symbol}[m]$ and structured as:

$$s_{d\_symbol}[m] = a + jb \tag{4.2}$$

$$m = 0,1,2..,(N_{samples}-1)$$

Where $a, b \in \{\pm 1, \pm 3, \dots, \pm(\sqrt{M}-1)\}$. The self-interference symbols are modulated similarly to the desired symbols in (4.2). To normalize the power of the symbols in (4.2) the total energy from the symbols is denoted as E and calculated

as the sum of each squared symbol. For m constellation points, the total energy is given as:

$$E = \sum_{i=1}^{m} \left(a_{I,i}^2 + b_{Q,i}^2\right) \tag{4.3}$$

Where $a_{I,i}, b_{Q,i}$ are the imaginary (I) and quardature (Q) components of the signaling points, respectively. Hence the average energy E_M is calculated as:

$$E_M = \frac{E}{K} \tag{4.4}$$

Hence the modulated symbols in (4.2), are scaled by the normalization factor $\frac{1}{\sqrt{E_M}}$, then the normalized modulated desired symbol $s_{d\_symbol\_n}[m]$ is represented as:

$$s_{d\_symbol\_n}[m] = \frac{1}{\sqrt{E_M}}\, s_{d\_symbol}[m] \tag{4.5}$$

$$m = 0,1, \dots, N_{samples} - 1$$

And the self-interference symbols are similary normalized.

4.2.1.3 Zero Padding

Zero paddings raise to the practice of adding zeros at the end of the time domain signal to increase its length. The purpose of this stage is to position invalid, null samples in the OFDM signal. Null samples are placed on the edge of the band to tolerate for simple extraction of the information samples. Since the IFFT/FFT size equals to 2048 samples, and the number of samples is 1200, an array of interleaved symbols is padded with nulls to form an array of 2048 samples [13]. From (4.5), we get the desired signal, which is denoted as $s_{d\_zp}[k]$ and zero padded as:

$$s_{d\_zp}[k] = 424\ nulls + \frac{s_{d\_symbol\_n}[m]}{2} + \ DC\ sample +$$

$$+ \ \frac{s_{d\_symbol\_n}[m]}{2} \ + \ 423\ nulls \tag{4.6}$$

Where the DC carrier stands for Direct Current, and it is a sample that has no information sent on it [3]. And k= $0,1, \dots, \mathrm{N_{FFT}} - 1$. The self-interference signal is zero padded similarly.

4.2.1.4 Inverse Fast Fourier Transform IFFT

The output of the zero paddings is the input for the IFFT, which is 2048. The IFFT converts the transmitted signal from the frequency domain to the time domain; then the time domain samples are sent as OFDM symbols over the transmitter. Hence the number of subcarriers is less than the size of the IFFT. The power of the IFFT must be normalized so that the average energy of IFFT is normalized. Furthermore, the normalization scaling factor f is given as:

$$f = N_{FFT} / \sqrt{N_{samples}} \tag{4.7}$$

Therefore, the total energy of 2048 symbols (including zero paddings) equals the power of 1200 as the 1200 samples carry the information. From (4.7) the input-output expression for the IFFT of the desired signal in the time domain is given as:

$$s_{d\_ifft}[\mathrm{n}] = \frac{1}{N_{FFT}} \sum_{t=0}^{N_{FFT}-1} e^{\frac{i2\pi kn}{N_{FFT}}} s_{d\_zp}[k] \tag{4.8}$$

Where $n = 0,1,2, \ldots, \mathrm{N_{IFFT}} - 1$ and the input-output for the IFFT of the self-interference signal in the time domain is corosspondgly to the desired signal in (4.8). Hence the desired signal in the time domain in (4.8) is scaled by the scaling factor from (4.7) as:

$$s_{d\_ifft\_n}[n] = f \times s_{d\_ifft}[n] \tag{4.9}$$

Where the × term represtns mulitplcation, and the self-interference signal is corosspondgly normlaized.

4.2.1.5 Cyclic Prefix Addition

The cyclic prefix is formed so that each OFDM symbol is headed by a copy of the end part of that equivalent symbol. In 4G LTE, a standard length and an extended length are obtainable, and after Release 8, a third extended length is also counted in [3]. The cyclic prefix addition is applied for the desired symbols, and the self-interference symbols after the IFFT process for each desired and self-interference OFDM symbol, the desired symbols noted as $\mathrm{s_{cp}}$:

$$s_d[t] = s_{d_i fft_n}[n + N_{cp}] \tag{4.11}$$

$$t = 0,1,2 \ldots., (N_{FFT} + N_{cp}) - 1$$

4.2.1.6 Convolution

The convolution process is formed for each OFDM symbol with each Rayleigh channel tap impulse response. This helps in exploiting the role of adding a cyclic prefix. The convolution is converted from linear to circular form for simple frequency domain equalization [36]. Referring to (2.6) the signal at the receiver represented as:

$$y[t] = h[t] * s_d[t] + g[t] * s_{si}[t] + z[t] \tag{4.11}$$

Where the term * represents the convolution and y[t] is given with a length of $t = 0,1,2 \ldots., (\mathrm{N_{FFT}} + \mathrm{N_{cp}}) - 1$, $h[t]$ and $g[t]$ are a Rayligh channel impulse response for the desired and self-interference channels respectively, and $y[t]$ denotes the full-duplex signal at the receiver.

4.2.2 Full-Duplex Reception

4.2.2.1 Remove Cyclic Prefix and Channel Taps

The N_{cp} cyclic prefix samples are deleted from the beginning of each received full-duplex OFDM symbol. As the channel is considered known at the full-duplex receiver.

In the full-duplex receiver, the cyclic prefix samples are deleted from the received signal $y[t]$. Hence, the receiver extracts the transmitted full-duplex signal $y[n]$ as:

$$y[n] = y(t - N_{cp}) \ + z\left(t - N_{cp}\right) \tag{4.12}$$

4.2.2.2 Fast Fourier Transform FFT

In this stage, the signal is converted from the time domain to the frequency domain where FFT renovates a cyclic time domain signal into its corresponding frequency spectrum [36]. As mentioned earlier, after the removal of the cyclic prefix, each OFDM symbol is of NIFFT length (2048 samples). The output after the removal of the cyclic prefix is then fed to the FFT block. Hence the FFT for $y[k]$ is expressed as:

$$y[k] = \sum_{t=0}^{N-1} e^{\frac{i2\pi kt}{N_{FFT}}} y[n] \tag{4.13}$$

$$k = 0,1,2, \ldots, N_{FFT} - 1$$

Where $y[k]$ denotes the received full-duplex OFDM symbols in the frequency domain.

The power normalization in FFT differs from the normalization in IFFT stage, in FFT the signal is normalized to the power of 1 by scaling $y[k]$ by the given factor:

$$y[k] = 1/f \times y[k] \tag{4.14}$$

4.2.2.3 Self-Interference Cancelation

Exploiting the FFT properties and demonstrating the role of the cyclic prefix that we mentioned before, the linear convolution of the OFDM symbols and the channel impulse response becomes a circular convolution [36]. After the (FFT) operation of OFDM, symbols at the full-duplex receiver are given by:

$$y[k] = h[k] * s_d[k] + g[k] * s_{si}[k] + z[k] \tag{4.15}$$

Where $s_d[k], s_{si}[k]$ denotes the desired OFDM symbols in the frequency domain and the generated OFDM self-interference symbols in the frequency domain, respectively. Correspondingly, $h[k], g[k]$ represent the desired Rayleigh in the frequency domain and the Rayleigh self-interference channel in the frequency domain. $z[k]$ denotes the noise samples in the frequency domain.

As proposed in the synchronization method, the $s_d[k]$ and $s_{si}[k]$ reference starting index is detected. Hence the self-interference symbols $s_{si}[k]$ and the self-interference channel $g[k]$ is canceled by subtracting $s_{si}[k]$ and $g[k]$ from $y[k]$; hence, $y[k]$ is obtained as:

$$y[k] = h[k] * s_d[k] + z[k] \tag{4.16}$$

4.2.2.4 Channel Equalization

One of the features of OFDM is that the channel estimation complexity is reduced as OFDM divides the available bandwidth into sub-channels [36]. Inside the sub-channels, each individually modulated OFDM symbol experiences the fading channel as flat fading. This opens up the option of operating a simple frequency domain equalizer to equalize the channel effects in the individual sub-channels [36]. The channel response $h[k]$ is assumed to be known at the receiver. Therefore, the channel effects are equalized at the receiver by applying a simple frequency domain equalizer. Hence, the estimated OFDM symbols in the subcarriers $s_d[k]$ are obtained by multiplying the frequency response of the received symbols $y[k]$, with the invert of the estimated channel response $h^{-1}[k]$. Then the desired symbol $s_d[k]$ is extracted as:

$$s_d[k] = \frac{y[k]}{h[k]} \tag{4.17}$$

4.2.2.5 Information Samples Extraction

As the information subcarriers are located around the DC carrier and the desired signal $s_d[k]$ is in the frequency domain, the information subcarriers are simply extracted by deleting the padded nulls. Furthermore, after removing the padded invalid nulls, the extracted desired symbols can be represented as $s_d[m]$, where $m = 0,1, \dots, (\mathrm{N}_{\mathrm{samples}} - 1)$

The desired symbols $s_d[m]$ only contain the $\mathrm{N}_{\mathrm{samples}}$ information subcarriers. Before demodulation, it is crucial to normalize the signal power by scaling it with the square root of the average energy E_M in (4.4), given as:

$$y[m] = \sqrt{E_M}\,(s_d[m]) \tag{4.18}$$

Where $y[m]$ are the normalized, received modulated complex symbols with length $=\mathrm{N}_{\mathrm{samples}}$.

4.2.2.6 Demodulation

As QPSK and MQAM modulation schemes are used in the OFDM transmitter, an optimum coherent detector on IQ plane using minimum Euclidean distance is operated to demodulate the received, modulated complex symbols [29]. The IQ detection technique is performed by modulating IQ reference array, accordingly, to the used modulation type and order, as shown below:

$$reference[M] = I_{ref} + Q_{ref} \tag{4.19}$$

Where M is the modulation order and of length $M = 0,1, \dots, \mathrm{M} - 1$.

The reference contains the ideal constellation points that are represented in the complex IQ plane, I_{ref} is the ideal real constellation reference point, and Q_{ref} represents the ideal imaginary constellation reference points.

The full-duplex transmitter and receiver agree on the same generated reference constellation for modulation and demodulation [36]. The Euclidean distance is implemented as a measure of the difference between the noisy received symbols and the modulated IQ reference array [29]. Therefore, the received symbols are converted from parallel to serial stream and the output received symbol $y[m]$ is given as:

$$y[m] = a_I[m] + jb_Q[m] \tag{4.20}$$

Where a_I represent the received real data symbols, and b_Q denote the received imaginary information symbols. And $m = 0,1, \dots, \mathrm{N}_{\mathrm{samples}} - 1$

For optimum coherent detection, the minimum squared Euclidean distance between the received noisy symbols $y[m]$ and the reference array $reference[M]$ is found and computed by comparing each a_I received vector with its corresponded reference I_{ref}, and comparing each b_Q received vector with its corresponded referenceQ_{ref}. The squared Euclidean distance d_{Eu} is computed as:

$$d_{Eu}[M,m] = \left\{\left(a_I[M,m] - I_{ref}\right)^2 + \left(b_Q[M,m] - Q_{ref}\right)^2\right\} \qquad (4.21)$$

The minimum distance for each received symbol index m is expressed as:

$$d_{min} = min_{\{N\}}(d_{Eu}[M,m]) \qquad (4.22)$$

Therefore, the receiver decides the symbols which are nearest ti the ideal value, and are equivalent to the originally transmitted symbols. Hence the received information OFDM symbol is expressed as:

$$\hat{r}[m] = a + jb \qquad m = 0,1,\dots,N_{samples} - 1 \qquad (4.23)$$

4.3 Simulation Results

4.3.1 Synchronization Peak

The detection of the reference OFDM symbol occurs by finding the index of the maximum value of the cross-correlation. Fig 4.1 illustrates the maximum value of the cross-correlation for the desired signal and self-interference signal, respectively. The starting index for the desired and the self-interference signals are at the sample index, where the maximum peaks are.

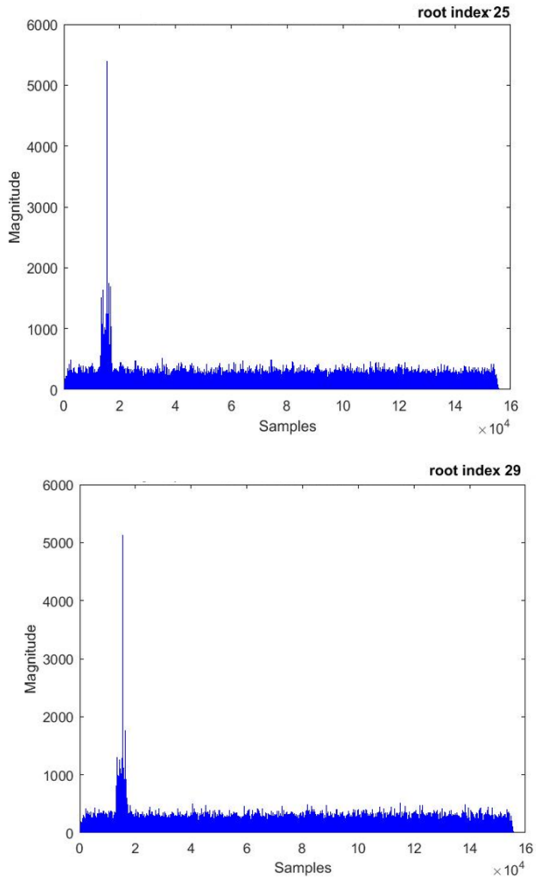

Fig. 4.1. Desired Signal NSP (with root Index 25) peak value and Self-Interference NSP (with root Index 29) peak value depending on the channel quality.

4.3.2 Successful Synchronization Probability (SSP)

As discussed in the previous chapter, SSP is the probability when the maximum peaks, which are detected by the cross-correlation, are at the correct sample index. The right sample index is the first sample of the OFDM symbol following the PSS symbol. The accurate index here is 15360. The desired SNR at the transmitter is

considered in the range of 0 to 40 dB, refereeing to figure (2.6) the digital residual self-interference $\mathrm{SNR_{si}}$ at the transmitter is assumed 40 dB.

Table 4.2. The percentage of the calculated cross-correlation maximum peaks at the correct sample index (15360)

$\mathrm{SNR_d}$	$\mathrm{SNR_{si}}$	Success Correlation Prob. (desired signal)	Success Correlation Prob. (SI signal)
0	40	0%	98%
10	40	0%	97%
20	40	3%	94%
30	40	30%	76%
40	40	63%	36%

From table 4.2, SNR_{si} denotes the self-interference signal power, and 1000 access trials, the analysis is discussed in the following 3 cases:

I. Case 1: When $\mathrm{SNR_d}$ is 0 dB, 10dB, and 20 dB, the successful correlation probability for the desired signal is at a maximum of 3%. Whereas, the SSP of the self-interference signal is above 90%. Hence the receiver uses the reference starting index of the self-interference signal. As seen above, 90% successful synchronization is achieved. Furthermore, the self-interference threshold value $\alpha_{th}^{(2)} = 20$ is optimized as the average result NSP value corresponding to the self-interference signal at the 20% access trial and the 25% access trial, as shown in Table 4.3.

Table 4.3. The average NSP corresponding to the desired and self-interference signal of the result values at the 20% access trial and the 25% access trial, according to the SNR in case 1

$\mathrm{SNR_d}$	$\mathrm{SNR_{si}}$	Desired signal NSP	Self-interference signal NSP
0	40	6	20.3
10	40	6.1	20.1
20	40	6.4	19.7

II. Case 2: In this case, when the desired SNR is 30 dB, the SSP for the desired signal increases to 30%, whereas, the SSP for the self-interference signal decreases to 76% SSP. In this case, around 30% successful synchronization of the desired signal is achieved, and 76% for the self-interference signal is achieved. Although the self-interference signal is still dominant, the receiver synchronization performance is better than in case 1, as the starting reference index of both signals can be detected at the receiver. Furthermore, in this case, the desired threshold value $\alpha_{th}^{(1)} = 8.9$ is optimized by the NSP values equivalent to the desired signal, as shown in table 4.4.

Table 4.4. The average NSP corresponding to the desired and self-interference signal of the resulting values at 20% access trial and 25% access trial, according to the SNR in case 2

SNR_d	SNR_{si}	Desired signal NSP	Self-interference signal NSP
30	40	8.9	17.3

III. Case 3: When the desired SNR equals SNR-SI, SCP for the desired signal increases to 63%, while SSP for self-interference decrease to 36%. SSP can differ around 3% at each simulation implementation. In this case, the desired signal is dominant. However, similar to case 2, both the signal's starting reference index can be detected at the receiver.

Table 4.5. The average NSP corresponding to the desired and self-interference signal of the resulting values at 20% access trial and 25% access trial, according to the SNR in case 3

SNR_d	SNR_{si}	Desired signal NSP	Self-interference signal NSP
40	40	15.7	11.2

4.3.3 Peak detection Probability

The performance results of successfully detected NSP probability, false alarm detected NSP probability, and not detected NSP probability for the NSP based desired signal corresponding to the desired threshold value$\alpha_{th}^{(1)} = 8.9$are shown in table 4.6. According to the proposed NSP based synchronization method, after the receiver detects the desired signal following case 2 and case 3, only 19% and 7% is not detected from the desired signal at the desired SNR 30 and 40dB.

Table 4.6. The NSP based synchronization probability for the desired signal and desired threshold value α_th^((1))=8.9 at the desired SNR range 0, 10, 20, 30, and 40 dB

$\mathbf{SNR_d}$	0	10	20	30	40
Success Detected Prob	0 %	0 %	1%	26%	63%
Not Detected Prob.	71%	79%	49%	19%	7%

Table 4.7. The NSP based synchronization probability for the self-interference signal and self-interference threshold value α_th^((2))=20 at the desired SNR range 0, 10, 20, 30, and 40 dB

$\mathbf{SNR_d}$	0	10	20	30	40
Success Detected Prob.	82%	80%	78%	62%	26%
Not Detected Prob.	18%	20%	22%	31%	50%

Table 4.7 shows the performance result of successfully detected NSP probability, false alarm detected NSP probability and not detected NSP probability, for the NSP based desired signal corresponding to the self-interference threshold value $\alpha_{th}^{(2)} = 20$. According to the proposed NSP based synchronization method following case 1, only 18%, 20% and 22% undetected probability of the self-interference signal is seen at the desired SNR 0, 10 and 20dB.

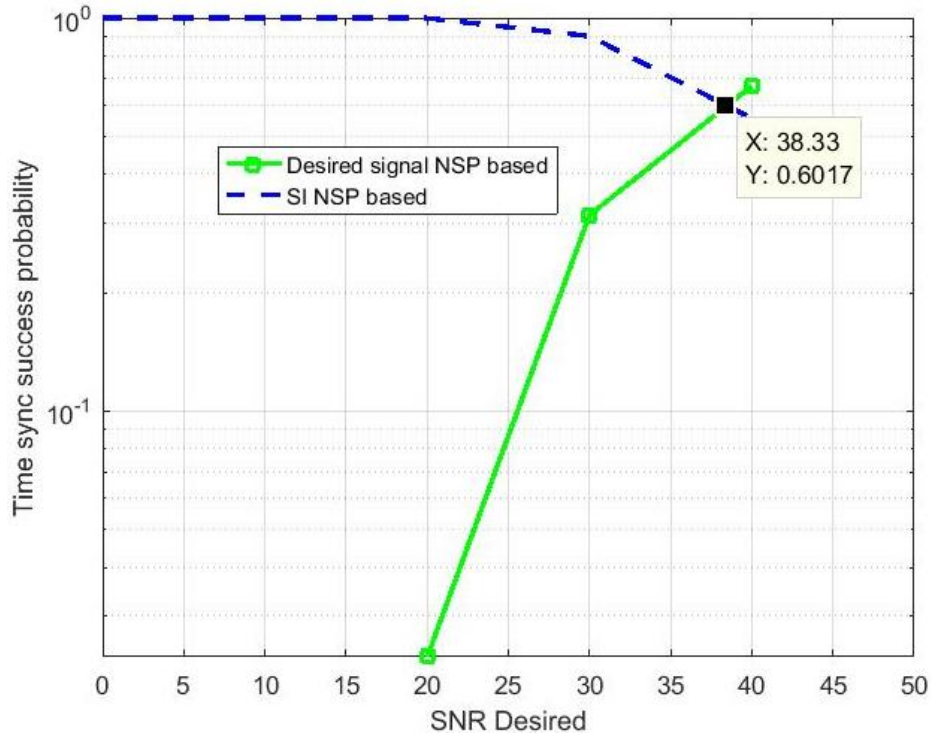

Fig. 4.2. Successful synchronization probability performance of full-duplex synchronization according to NSP based desired and self-interference signals.

For the performance measurement, 1000 access trials were simulated. The desired SNR range is from 0 to 40 dB, the Self-interference SNR is 40 dB, and the desired and self-interference signals are OFDM QPSK modulated.

Fig 4.2 shows the successful probability performance of the simulated full-duplex synchronization when NSP based synchronization method is used. As in case 1 and case 2, when the desired SNR is low, corresponding to the self-interference SNR, Successful synchronization probability is achieved by exploiting the PSS of the self-interference signal. While the desired SNR equals to the self-interference SNR (case 3), successful synchronization probability operating the PSS of the desired signal is better.

As a result, the proposed NSP based synchronization method yields approximately 90% successful synchronization probability in all SNR regions according to the NSP based desired and self-interference signals. Minimum successful synchronization probability is 60% at the desired SNR of 38dB. The crossing point, where the NSP based desired signal and NSP based self-interference signal intersect, is located within high desired SNR of 30 and 40dB. Hence,

synchronization occurs by selecting the NSP index according to the self-interference PSS; this is because the self-interference SNR is too high.

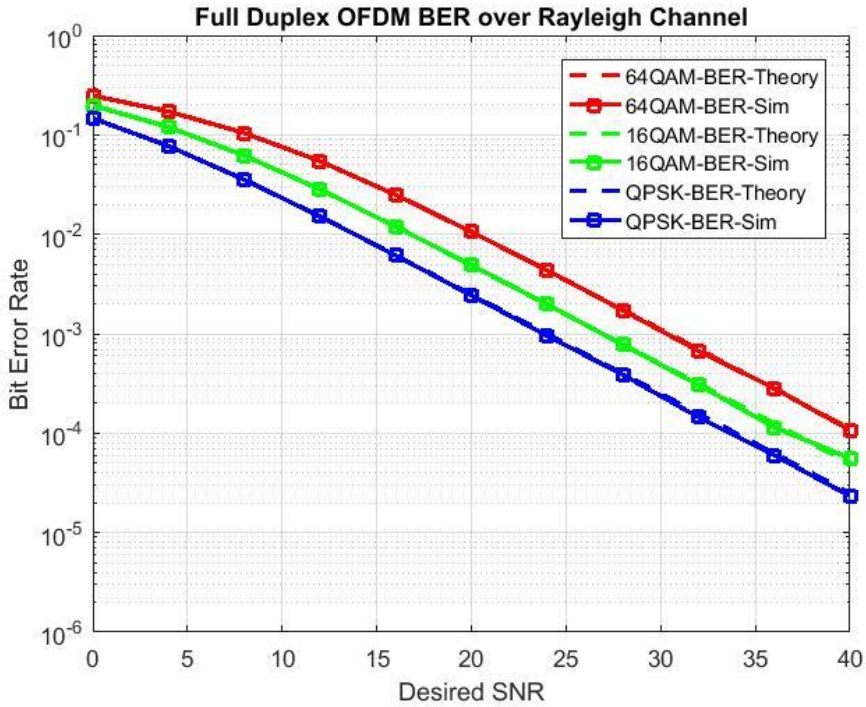

Fig. 4.3. Full-Duplex BER Performance

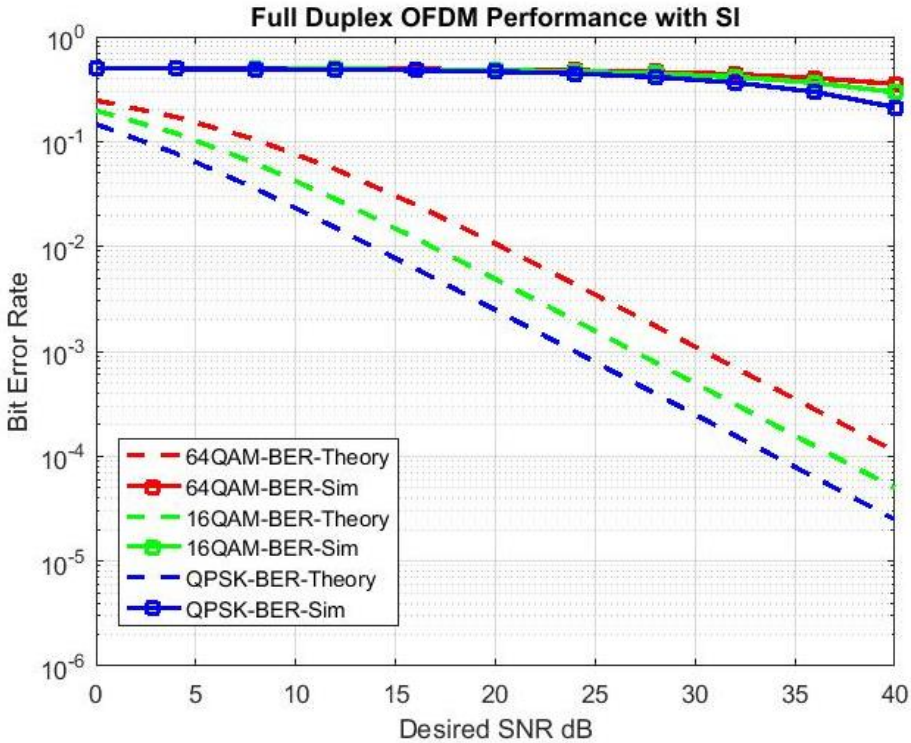

Fig. 4.4. Full-Duplex BER Performance with the effect of the self-interference signal.

Fig 4.3 shows the OFDM Full-duplex transceiver BER for OFDM QPSK, 16QAM and 64QAM modulation for the desired and self-interference signals over a 10 tap Rayleigh channel. As a result, the simulated BER for all modulations is correspondent to the theoretical BER, which means that the self-interference signal is successfully canceled from the desired received signal by the proposed full-duplex simulation. The effect of the self-interference signal on the desired signal can be seen in Fig 4.4, where the desired signal BER is very high, resulting in high distortion caused by the interference.

CHAPTER 5

5 Conclusion and Future work

In this thesis, a system design is proposed for the problem of self-interference cancellation in full-duplex communications. A system architecture design has been presented using spatial isolation and time synchronization for the cancellation of analog and digital self-interference. PSS signals were constructed and used to assist in the detection performance of the signal. For the performance measurement, 1000 access trials were simulated, the desired SNR range was from 0 to 40 dB, the Self-interference SNR is 40 dB, and the desired and self-interference signals were OFDM QPSK modulated.

A full-duplex radio innovation is crucial for expanding the spectrum efficiency, mainly, when the user demand is increasing tremendously, and the radio resources are limited and restricted. A time synchronization method for full-duplex communication is proposed based on a novel optimization approach for the NSP threshold values, for both the desired and self-interference signal.

As a result, the proposed NSP based synchronization method yields approximately 90% successful synchronization probability in all SNR regions, according to the NSP based desired and self-interference signals. The proposed method is verified by simulating OFDM full-duplex transceiver in MATLAB, and the simulation proves a minimum of 60% time synchronization success rate by the proposed NSP based synchronization method, which is expected to be a useful reference for future work and studies.

OFDM Full-duplex transceiver is simulated, and the performance is verified by the Bit Error Rate (BER). It is expected that this simulation delivers a valuable understanding and contribution to the emerging future of full-duplex radio.

For future work, modifications will be made to enhance the system performance using better equipment. Higher accuracy and a more stable system can be achieved by introducing state of the art hardware equipment. However, we believe that this thesis can be further developed to be physically exploited to achieve 5G communication.

References

[1] 3GPP, “An Introduction to LTE,” *3GPP,* vol. 3GPP LTE Encyclopedia, 2010.

[2] Motorola, "Long Term Evolution (LTE): A Technical Overview," *TECHNICAL WHITE PAPER,* 2010.

[3] D. Erik, S. Parkvall and J. Sköld, 4G-Advanced Pro and The road to 5G, 3rd ed., vol. I, London: Elsevier Ltd, 2016, pp. 1-5.

[4] A. F.Molisch, Wireless Communication, London: Willy, 2011.

[5] A. Nordrum, K. Clark and I. S. Staff, 5G Bytes: Millimeter Waves Explained, spectrum.ieee.org, 2017.

[6] Sprint.com, "Sprint Unveils Six 5G-Ready Cities; Significant Milestone Toward Launching First 5G Mobile Network in the U.S.," February 27, 2018.

[7] J. Mundy, "What Is Massive MIMO Technology?," *5g.co.uk,* p. 1.

[8] E. G. Larsson, O. Edfors, F. Tufvesson and T. L. Marzetta, "Massive MIMO for next generation wireless systems," *IEEE communications magazine,* vol. 52, pp. 196-195, March 2014.

[9] Ericsson, "Ericsson Mobility Report Q4 2018 Update," *Ericsson Mobility Report,* pp. 1-4, 2019.

[10] National Institute of Standards and Technology, "The Spectrum Crunch," 05 February 2019. [Online]. Available: https://www.nist.gov/topics/advanced-communications/spectrum-crunch. [Accessed 05 February 2019].

[11] G. R. Kenworthy, "Self-cancelling full-duplex RF communication system," USPTO, 1997.

[12] D. Bharadia, E. McMilin and S. Katti, "Full Duplex Radios," *Stanford University,* pp. 50-62, August 2013.

[13] M. Chung, M. S. Sim, J. Kim and C. B. Chae, "Prototyping Real-Time Full Duplex Radios," *IEEE Communications Magazine,* vol. 53(9), pp. 56-63, September 2015.

[14] P. J. Zhang, D. G. d. l. Roche, A. Valcarce, D. Lopez, E. Liu and H. Song, Femtocells — Technologies and Deployment, Wiley, 2010.

[15] J. Kim, M. S. Sim, M. Chung, D. K. Kim and C.-B. Chae, "Full-duplex Radios in 5G: Fundamentals, Design and Prototyping," in *Signal Processing for 5G: Algorithms and Implementations*, Wiley-IEEE Press, 2016, pp. 539-560.

[16] M. Chung, M. S. Sim, D. K. Kim and C. B. Chae, "Compact Full Duplex MIMO Radios in D2D Underlaid Cellular Networks: From System Design to Prototype Results," *IEEE Access,* vol. 5, pp. 16601-16617, 2017.

[17] D. Bharadia, E. McMilin and S. Katti, "Full Duplex Radios," *ACM SIGCOMM,* pp. 375-386, 2013.

[18] A. Ghosh, J. Zhang, J. G. Andrews and R. Muhamed, Fundamentals of LTE, Prentice

Hall, 2010.

[19] S. C. Cripps, RF Power Amplifers for Wireless Communications, Artech House, 1999.

[20] Y. Suzuki, S. Narahashi and T. Nojima, "Evaluation of non-linear compensation effect of base station power amplifier on adjacent channel interference between different mobile systems," *2010 IEEE International Conference on Communication Systems,* 17-19 11 2011.

[21] H. Steven, B. Joel, C. Jung, J. Mayank, M. Jeff, K. Sachin and L. Philip, "Applications of self-interference cancellation in 5G and beyond," *IEEE Communications Magazine,* vol. 52(2), pp. 114-121, 2018.

[22] J. I. Choi, M. Jain, K. Srinivasan, P. Levis and S. Katti, "Achieving single channel, full duplex wireless communication," *Stanford University,* pp. 20-24, 2010.

[23] D. Korpi, M. AghababaeeTafreshi, M. Piilila, L. Anttila and M. Valkama, "Advanced architectures for self-interference cancellation in full-duplex radios: Algorithms and measurements," *2016 50th Asilomar Conference on Signals, Systems and Computers,* no. 16723870, 2016.

[24] S. Hong, J. Brand, J. I. Choi, M. Jain, J. Mehlman, S. Katti and P. Levis, "Applications of Self-Interference Cancellation in 5G and Beyond," *IEEE Communications Magazine,* vol. 52, pp. 114-121, 2014.

[25] M. Duarte, C. Dick and A. Sabharwal, "Experiment-Driven Characterization of Full-Duplex Wireless Systems," *IEEE Transactions on Wireless Communications,* vol. 11, pp. 4296-4307, 2012.

[26] E. Aryafar, M. (. khojastepour, K. Sundaresan, S. Rangarajan and M. Chiang, "MIDU: Enabling MIMO Full Duplex," *MobiCom'12,* no. 978-1-4503-1159-5, pp. 22-26, 2012.

[27] A. K. Khandani, Full-duplex (Two-way) Wireless: Antenna Design and Signal Processing, Toronto, ON, Canada: University of Waterloo, 2013.

[28] M. Chung, L. Liu, O. Edfors, D. K. Kim and C. B. Chae, "Robust timing synchronization for full duplex communications: Design and implementation," *IEEE Global Conference on,* pp. 883-887, 8 March Nov, 2017.

[29] G. Lindell, Introduction to Digital Communication, Lund: Lund University, 2006.

[30] G. Lindell, "An introduction to OFDM, V 161115," lecture notes in the course digital communication advanced course (ETTN01), Lund.

[31] S. Sesia, I. Toufik and M. Baker, LTE: the UMTS long term evolution, New York: John Wiley & Sons, 2009.

[32] Z. Hans Jurgen and A. Finger, Pseudo Random Signal Processing: Theory and Application, John Wiley & Sons, Ltd, 2013.

[33] R. Bracewell, "Pentagram Notation for Cross Correlation," in *The Fourier Transform and Its Applications*, New York, 1965, pp. 46-243.

[34] T. R. Pechetty and M. Vemulapalli, "An Implementation of OFDM Transmitter and Receiver on Reconfigurable Platforms," *International Journal of Advanced Research in Electrical, Electronics and Instrumentation Engineering,* vol. 2, no. 11, pp. 5486, 5487, 5488, 2013.

[35] M. Viswanathan, Digital Modulations Using Matlab: Build Simulation Models from Scratch, Amazon Digital Services LLC, 2017.

[36] M. Viswanathan, Digital Modulations using Matlab, 2017.

[37] 3GPP, "3GPP Portal," *portal.3gpp.org,* vol. Portal, 2016.

[38] T. H. Lee, The Design of CMOS Radio-Frequency Integrated Circuits, Second Edition, Cambridge University, 2003.

[39] M. S. Sim, M. Chung, D. Kim, J. Chung, D. K. Kim and C. B. Chae, "Nonlinear Self-Interference Cancellation for Full- Duplex Radio: From Link and System-Level Performance Perspectives," *IEEE Communications Magazine,* vol. 55(9), pp. 158-167, 2017.

[40] Ericsson, "White Paper: LTE – an introduction," *Ericsson Report,* June 2019.

Series of Master's theses
Department of Electrical and Information Technology LU/LTH-EIT
2018-628 http://www.eit.lth.se

Printed by Tryckeriet i E-huset, Lund 2019

LUND
UNIVERSITY

Series of Master's theses
Department of Electrical and Information Technology
LU/LTH-EIT 2019-734
http://www.eit.lth.se